UV Photochemistry of Thin Film and Matrix-Isolated Acetyl Chloride by Polarized FTIR

Brad Rowland[†] **and Wayne P. Hess***

Environmental Molecular Sciences Laboratory, Pacific Northwest National Laboratory, P.O. Box 999, Richland, Washington 99352

Received: June 17, 1997; In Final Form: September 3, 1997[⊗]

A concerted HCl elimination reaction is observed following ultraviolet photoexcitation of neat and matrix-isolated samples of acetyl chloride. The photoreaction of condensed-phase acetyl chloride forms HCl·ketene complexes exclusively, in sharp contrast to the gas-phase photoreaction that produces Cl atoms, CH_3CO, CH_3, and CO. The reaction mechanism involves photoexcitation followed by $S_1 \rightarrow S_0$ interconversion and a four-centered elimination on the ground electronic surface. The HCl·ketene complexes are the only primary photoproduct observed and are found to be aligned with the polarization axis of the irradiating laser. The polarization specific FTIR probe indicates that the HCl·ketene complexes form a T-shaped structure quite similar to the transition state structure recently calculated for HCl elimination from CH_3COCl.

Introduction

Studying the differences between gas- and condensed-phase photochemistry strengthens our understanding of many-body interactions in reactive processes. The photoreactivity of small molecules can be highly sensitive to phase, and well-known gas-phase reaction mechanisms are often modified in the condensed phase or completely subsumed by other distinct reactive channels. The extension of gas-phase results to heterogeneous surfaces, as is often done for reactions of relevance to combustion and atmospheric chemistries, and the interstellar medium[1−5] should therefore be applied with considerable caution. For example, the photochemistry of aldehydes and ketones proceeds by distinctly different mechanisms in gas and liquid phases. Ultraviolet excitation of acetone leads to fragmentation into CH_3 and CO in the gas phase but reacts by H-atom abstraction to form the propanol radical in the liquid phase.[6]

We have recently studied the condensed-phase photochemistry of acetyl chloride and found that the S_1 reaction mechanism in neat cryogenic films is entirely different from that of isolated (jet-cooled) molecules.[7] Here, we have extended these studies to further elucidate the details of the condensed-phase reaction mechanism. Ultraviolet (UV) gas-phase photodissociation of acetyl chloride proceeds through a two-step mechanism. Photoexcitation of the ∼5 eV $\pi^* \leftarrow$ n transition leads to rapid dissociation into chlorine atoms and acetyl radicals ($\tau < 1$ ps).[8−11] Roughly one-third of the newborn acetyl radicals contain sufficient energy to further fragment forming CO and CH_3.[12,13] This impulsive gas-phase dissociation occurs on an excited singlet surface that correlates to the ground electronic states of acetyl radicals and Cl atoms (both ground Cl ($^2P_{3/2}$) and spin−orbit excited Cl* ($^2P_{1/2}$) atoms are produced). The initial excited singlet state apparently evolves from the (C═O)* configuration into a (C−Cl)* antibonding configuration, entirely on singlet surfaces,[14−16] although there is debate over the details of the excited-state evolution.[8,14,16] Presumably, the energetic proximity of the relevant diabatic singlet states promotes the rapid evolution to the repulsive (C−Cl)* configuration.

Since the gas-phase reaction proceeds initially by rapid dissociation of the C−Cl bond, it is reasonable to postulate that the first step in the condensed-phase photoreaction also involves C−Cl bond cleavage as described in reactions 1 and 2:

$$[CH_3COCl] + h\nu \rightarrow [CH_3COCl\ (S_1)] \quad \text{(photoexcitation)} \tag{1}$$

$$[CH_3COCl\ (S_1)] \rightarrow [Cl_t + H_3CCO^{\#}] \quad \text{(caged dissociation)} \tag{2}$$

Here, the Cl_t represents the newborn Cl radical with translational motion and the $H_3CCO^{\#}$ represents the acetyl radical with both internal excitation and translational motion. The square brackets denote the matrix cage. Extrapolating this line of reasoning, we consider possible subsequent reactions 3−5:

$$[Cl_t + H_3CCO] \rightarrow [HCl + H_2C{=}C{=}O] \quad \text{(abstraction/disproportionation)} \tag{3}$$

$$[Cl_t + H_3CCO] \rightarrow [CH_3Cl + CO] \quad \text{(CO displacement)} \tag{4}$$

$$[Cl_t + H_3CCO] \rightarrow [CH_3COCl^{\#}\ (S_0)] \quad (S_0 \text{ recombination}) \tag{5}$$

Unlike the gas-phase reaction, the condensed-phase reaction forms HCl and ketene exclusively. Since we do not observe methyl chloride formation as in reaction 4, it is possible that the condensed-phase reaction is not initiated by C−Cl bond cleavage. We therefore propose a second set of possible subsequent reactions 6−9:

$$[CH_3COCl\ (S_1)] \rightarrow [CH_3COCl^{\#}\ (S_0)] \quad \text{(internal conversion)} \tag{6}$$

$$[CH_3COCl\ (S_1)] \rightarrow [CH_3COCl\ (T_1)] \quad \text{(intersystem crossing)} \tag{7}$$

$$[CH_3COCl^{\#}\ (S_0)] \rightarrow [HCl + H_2C{=}C{=}O] \quad (S_0 \text{ elimination}) \tag{8}$$

$$[CH_3COCl\ (T_1)] \rightarrow [HCl + H_2C{=}C{=}O]^3 \quad (T_1 \text{ elimination}) \tag{9}$$

[†] AWU Postdoctoral Research Associate.
* Corresponding author. E-mail: wp_hess@pnl.gov.
[⊗] Abstract published in *Advance ACS Abstracts,* October 1, 1997.

S1089-5639(97)01980-4 CCC: $14.00

Recently, Sumathi and Chandra explored the potential energy surface of acetyl chloride in the electronic ground and lowest adiabatic triplet states using ab initio methods.[17] They examined a variety of reaction channels and found that (on the electronic ground state) elimination to form HCl and ketene was the most energetically favorable. The lowest triplet surface was also examined and found to have low-energy activation barriers (8−14 kcal/mol) for dissociation into a variety of radicals. Sumathi and Chandra calculated the ground-state barrier to HCl elimination to be 48 kcal/mol at the MP2/6-31G*//6-31G* level. Thermally activated HX elimination from alkyl halides has well-known activation energies that have been measured between ∼50 and 70 kcal/mol.[18−20] Toto et al. have calculated the transition-state structure and activation energies for 1,2-elimination of HCl from ethyl chloride. These calculations predict an activation energy of 61.6 kcal/mol, which is nearly 14 kcal/mol higher than that calculated for acetyl chloride.[21]

To distinguish among the possible condensed-phase reaction mechanisms, we probe the UV photochemistry of thin films of neat and matrix-isolated acetyl chloride following 266 and 193 nm irradiation. Several matrixes, such as Ar, Xe, O_2, and C_3H_8, are used to probe the effect of various neighboring species on the photolysis of acetyl chloride. For comparative purposes, thin films of Cl_2 isolated in a propane matrix are irradiated (at 355 nm) to verify the Cl/propane reaction within the cryogenic film.

Polarized Fourier transform infrared (FTIR) techniques have been used to assign vibrational modes of matrix-isolated phthalic anhydride[22] to study the cis-to-trans transformation of matrix-isolated butadiene[23] and to study the alignment of molecules adsorbed onto a surface.[24,25] In these previous studies, the orientation of vibrational dipoles relative to a laboratory axis was determined by evaluating the effects of polarization on the IR band intensities.[26] We use polarized FTIR spectroscopy to determine the orientation of all trapped product molecules with respect to the 266 nm UV laser polarization.

Experimental Method

Thin films of neat and matrix-isolated acetyl chloride are deposited onto KBr or BaF_2 substrates mounted to a closed-cycle helium cryostat. Neat samples are deposited from $\sim10^{-4}$ Torr vapor to a total thickness of ∼4 μm on a substrate held at 20 K (∼2 μm is deposited on each side of the substrate window). Deposits of neat acetyl chloride are crystallized by slowly warming (2 K/min) from 20 to ∼110 K, at which point the amorphous sample has crystallized. Following the amorphous-to-crystalline phase change, the sample is cooled to 11 K for FTIR analysis. Argon matrix-isolated thin films of acetyl chloride (500:1, Ar:CH_3COCl) are vapor deposited through a single nozzle (1.6 mm diameter) onto substrates at 11 K. Deposits of xenon matrix-isolated acetyl chloride molecules (300:1, Xe:CH_3COCl) are similarly prepared onto a substrate at 20 K. Thin films of acetyl chloride in O_2 and C_3H_8 (both 200:1) are vapor deposited through a single nozzle onto a substrate at 11 K. The temperature of the substrate is measured using a silicon diode attached directly to the substrate and is maintained within ±0.1 K by an autotuning temperature controller.

The thickness of film deposits is determined by optical interference measurements using a 633 nm helium−neon laser.[27] The helium−neon laser is aligned on the growing films at a near-normal angle, and the intensity of the reflected beam is monitored by a photodiode. The film thickness d is given by $d = [\lambda/(2n)]N$, where the index of refraction, the number of full optical interference oscillations, and the wavelength of the laser light are represented by n, N, and λ, respectively.[27] The film thickness of the xenon matrixes could not be measured because of the similar refractive indices of the KBr substrate ($n = 1.56$) and condensed xenon ($n = 1.50$) at 20 K (the index of refraction of condensed argon is 1.29 at 20 K).[28,29] We monitor the amorphous-to-crystalline phase transition of acetyl chloride using the same optical interference technique used to measure film thickness. As a neat sample is warmed, the intensity of the reflected beam changes dramatically between 103 and 107 K because of the change in density upon crystallization. Above 107 K, grain boundaries can form, between microcrystalline regions, such that the HeNe beam is severely scattered, eliminating the reflected beam. The thickness of neat, Ar, and O_2 matrix-isolated acetyl chloride samples is 1.8, 5.0, and 4.4 μm, respectively. The thickness of the propane film cannot be directly measured because of the refractive scattering of the reflected HeNe beam but is estimated to be ∼5 μm for acetyl chloride in propane and ∼2 μm for Cl_2 in propane.

We irradiated matrix-isolated acetyl chloride thin films using the 266 nm fourth harmonic of a Nd:YAG laser. Matrix-isolated Cl_2 thin films were irradiated using the 355 nm third harmonic of a Nd:YAG laser. Matrix samples used in photoproduct alignment studies are irradiated between 1 and 2 min using an average pulse energy of 0.3 mJ at a 20 Hz repetition rate with a 1.5 cm diameter beam. The vertically polarized UV laser can be rotated by using a half-wave plate, thus producing horizontally polarized light. A comparison of photoexcited samples using vertically and horizontally polarized light shows that the alignment of consumed acetyl chloride and photoproducts rotates 90° as expected. In studies designed to detect secondary photoproducts, matrix samples are irradiated for ∼3 h using an average pulse energy of 0.5 mJ at a 20 Hz repetition rate. Neat samples of acetyl chloride are typically irradiated for ∼30 min at an average pulse energy of 0.5 mJ. Selected samples were irradiated by ArF excimer emission at 193 nm using similar repetition rates and fluences.

Infrared spectra are collected before and after irradiation at a resolution of 2 cm^{-1} using a Mattson 10 000 FTIR spectrometer. Subtraction of the pre- and postirradiated spectra produces a "difference spectrum" that displays the newly formed products and the consumed CH_3COCl reactant. Polarized IR spectra are obtained by inserting an IR polarizer between the IR source and condensed sample. The orientation of the HCl·ketene complex is analyzed by collecting background and pre- and postirradiated FTIR spectra at 45° increments of the IR polarizer. Subtracting background spectra collected at each 45° increment removes any artifact associated with polarization sensitive optics within the FTIR spectrometer. In the low total irradiance experiments (designed to measure product orientation) less than 10% of the acetyl chloride sample is photoreacted. The assignments of the vibrational modes of acetyl chloride, ketene, and HCl are made from the literature values,[30−32] as are the assignments for other photoproducts produced in propane and xenon matrixes.[33−42]

Results

The infrared spectrum of HCl·ketene complexes formed following 266 nm irradiation of matrix-isolated acetyl chloride is displayed in Figure 1. Acetyl chloride is readily identified by the strong C═O stretch band at 1808 cm^{-1}, and similarly, the HCl·ketene photoproducts are identified by strong IR bands at 2685 cm^{-1} (HCl) and at 2145 cm^{-1} (C═O stretch). Com-

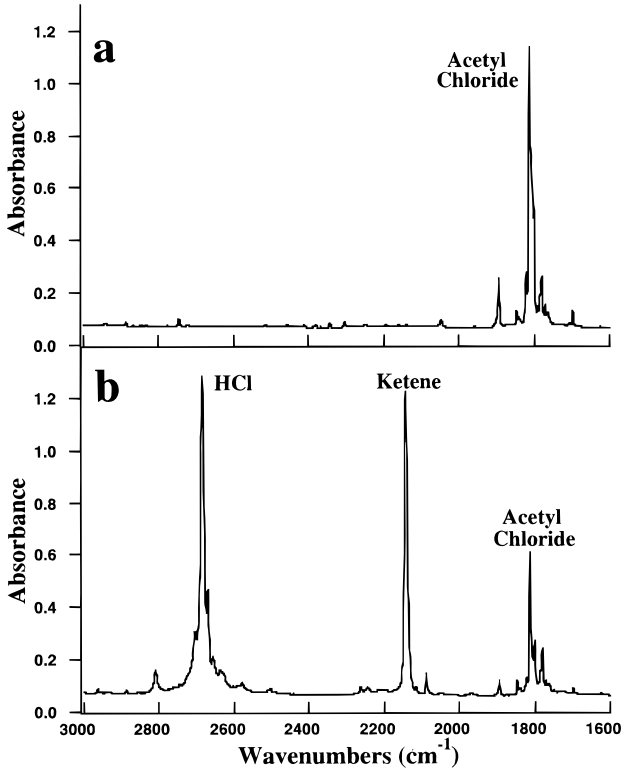

Figure 1. Infrared spectra of preirradiated (a) and postirradiated (b) samples of matrix-isolated (argon, 500:1) acetyl chloride at ~11 K. Assignments of the vibrational modes of acetyl chloride, HCl, and ketene are noted.

plexed HCl·ketene photoproducts are also observed in UV-irradiated films of neat and Xe matrix-isolated acetyl chloride.[7,43] No other primary photoproducts are observed. Figure 2 displays an expansion of the spectral region between 2940 and 3000 cm^{-1} showing the absence of the C−H stretch band indicative of CH_3-Cl product. Small amounts of *secondary* products CH_3Cl and CO are observed in argon matrix-isolated acetyl chloride but only after extensive UV irradiation at 266 nm.

Figure 3 displays a comparison of the FTIR spectra of irradiated neat and matrix-isolated acetyl chloride samples. Although the photoproducts in neat and matrix-isolated samples are identical, the IR spectra are quite different. The HCl band in the spectrum of the neat sample is strongly broadened (fwhm $\approx$ 250 cm^{-1}) because of the intermolecular coupling of HCl molecules with the surrounding acetyl chloride matrix. A relatively narrow IR band (fwhm $\approx$ 11 cm^{-1}) due to the much weaker argon−HCl interaction is observed for matrix-isolated HCl. The C═O stretch of ketene is also broadened in the neat sample (fwhm $\approx$ 25 cm^{-1}) compared to the matrix-isolated sample (fwhm $\approx$ 11 cm^{-1}). The band centers of the HCl and ketene, formed in the neat sample, are red-shifted from the argon matrix values by 40 and 13 cm^{-1}, respectively. Again, there is no indication of primary photoproducts other than HCl and ketene.

The pre- and postirradiated spectra of acetyl chloride in a propane matrix are displayed in Figure 4. The CH stretch and the CH_3 deformation regions in the IR spectra completely absorb the IR probe light. However, the formation of ketene and HCl from the photolysis of acetyl chloride (100% consumed) is still easily observed. Figure 4c displays the difference spectrum, clearly showing ketene and HCl as the primary photoproducts.

Figure 5 displays the difference spectrum of the reaction products formed following photoexcitation of Cl_2 in a propane matrix. The vibrational modes of HCl, propene (H_2C═$CHCH_3$),

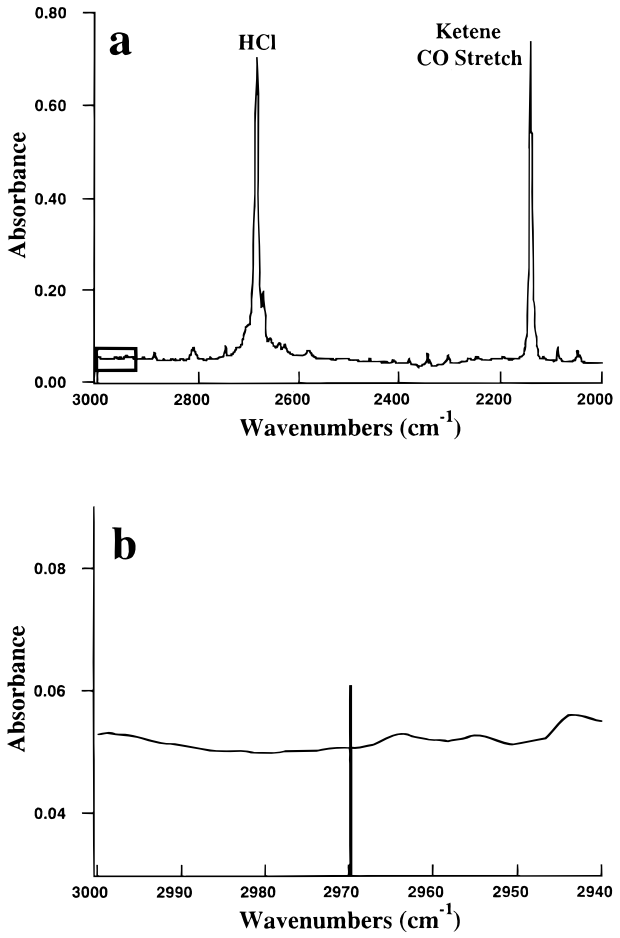

Figure 2. Difference FTIR spectra of HCl and ketene products in an argon matrix (a) with the 2940−3000 cm^{-1} region marked. No CH_3Cl is observed following 13% photoconversion of the sample as revealed in the expansion of the 2940−3000 cm^{-1} region. The expected position of the methyl chloride C−H stretch is marked by the vertical line (b).

2-chloropropane, and 1-chloropropane products are observed. The sharp C═C stretch of propene, located at 1640 cm^{-1}, is clearly evident in Figure 5. In this spectral region, no overlapping propane, ketene, or acetyl chloride absorptions interfere at 1640 cm^{-1} such that the band assignment is unambiguous. The assigned IR bands are listed in Table 1. None of the IR bands observed in Figure 5 (except those attributed to HCl) are observed in Figure 4c.

Parts a and b of Figure 6 show the difference spectra obtained following 193 nm irradiation of acetyl chloride in propane and xenon matrixes, respectively. The propene band is observed at ~1640 cm^{-1}, as are several other bands indicative of Cl reaction with propane. A comparison with Figure 5 reveals that both spectra display IR bands attributed to HCl, propene, and 2-chloropropane. Infrared bands attributed to other products, such as acetaldehyde and 2-chloroethanol, are listed in Table 2. Absorption bands of ketene, CH_3Cl, CO, and CH_3 products are observed following 193 nm irradiation of acetyl chloride isolated in a xenon matrix and are cataloged in Table 3. These results indicate that translationally excited Cl atoms indeed react within a propane matrix. Furthermore, caged Cl atoms are capable of methyl group abstraction to produce CH_3Cl and CO.

Three bands attributed to HCl are observed following 193 nm irradiation of xenon matrix-isolated acetyl chloride (Figure 6b). These bands centered at 2855, 2807, and 2661 cm^{-1} are assigned to isolated, semi-isolated, and complexed HCl, respectively. The frequency of isolated HCl agrees with the reported value for HCl doped into Xe matrixes (2853 cm^{-1}).[32] The

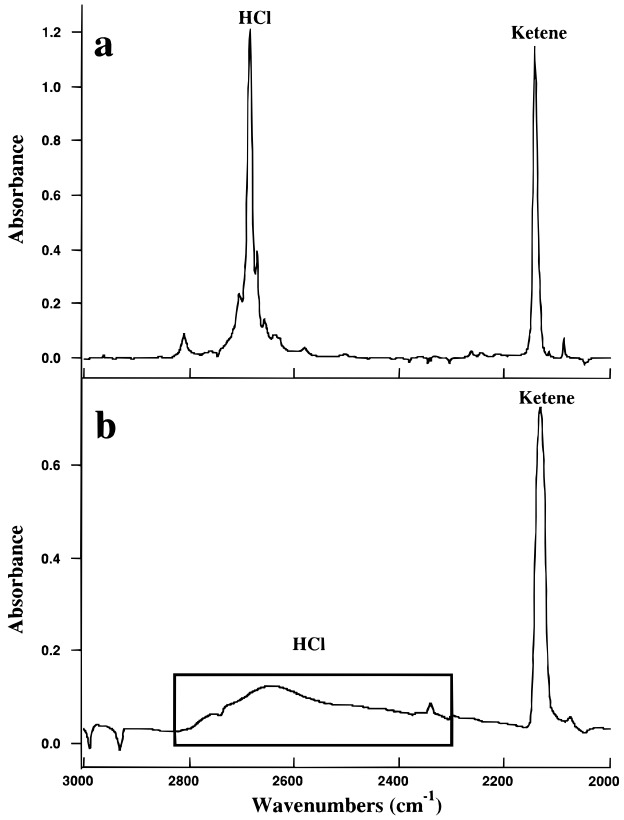

Figure 3. Infrared spectra of irradiated acetyl chloride in matrix-isolated (argon, 500:1) (a) and neat films (b). The fwhm of HCl and ketene bands are ∼11 cm^{-1} in the matrix-isolated sample, but the fwhm of HCl and ketene bands are ∼250 and 25 cm^{-1}, respectively, in the neat acetyl chloride sample. The spectra were obtained at a sample temperature of ∼11 K.

TABLE 1: Vibrational Frequencies (cm^{-1}) of the Photoproducts of 355 nm Irradiated Cl_2 in a Propane Matrix

assignments	observed frequency	literature frequency	mode[d]
propene[a]	3083	3091	ν(CH)
HCl	2770−2610		
propene	1640	1646	ν(C═C)
propene	1437	1435	$\delta_{as}(CH_3)$
1-chloropropane[b]	1303	1305	$\gamma(CH_2)$
2-chloropropane[c]	1259	1260	δ(CHCl)
2-chloropropane	1161	1161	$\rho(CH_3)$
2-chloropropane	1062	1062	$\rho(CH_3)$
propene	1045	1042	$\rho(CH_3)$
propene	1000	992	δ(CH)
propene, 2-chloropropane	926	934	$\rho(CH_2)$
		933	$\rho(CH_3)$
propene	916	910	$\delta(CH_2)$
2-chloropropane	886	887	ν(CC)
1-chloropropane	858	856	$\rho(CH_2)$
1-chloropropane	787	789	$\rho(CH_2)$
1-chloropropane	724	727	ν(C−Cl)

[a] Liquid propene assignments from ref 33. [b] Frequencies of liquid 1-chloropropane from ref 34; assignments from ref 35. [c] Liquid 2-chloropropane assignments from ref 36. [d] ν represents stretching modes, δ represents deformation or bending modes, ρ represents rocking or twisting modes, and γ represents waging modes.

frequency of complexed HCl is red-shifted ∼192 cm^{-1} from the reported Xe matrix-isolated value, which agrees with the ∼203 cm^{-1} shift observed for HCl complexed with ketene in an argon matrix. The frequency of the semi-isolated HCl is only red-shifted by ∼43 cm^{-1}, which indicates that the HCl molecule weakly interacts with the neighboring ketene molecule, as opposed to the complexed HCl that strongly interacts with its ketene neighbor. For HCl and ketene photoproducts of Xe matrix-isolated acetyl chloride at 266 nm, HCl located at the semi-isolated position (2807 cm^{-1}) has greater IR band intensity than that located at the complexed position (2661 cm^{-1}), indicating mobility of HCl within the Xe matrix.

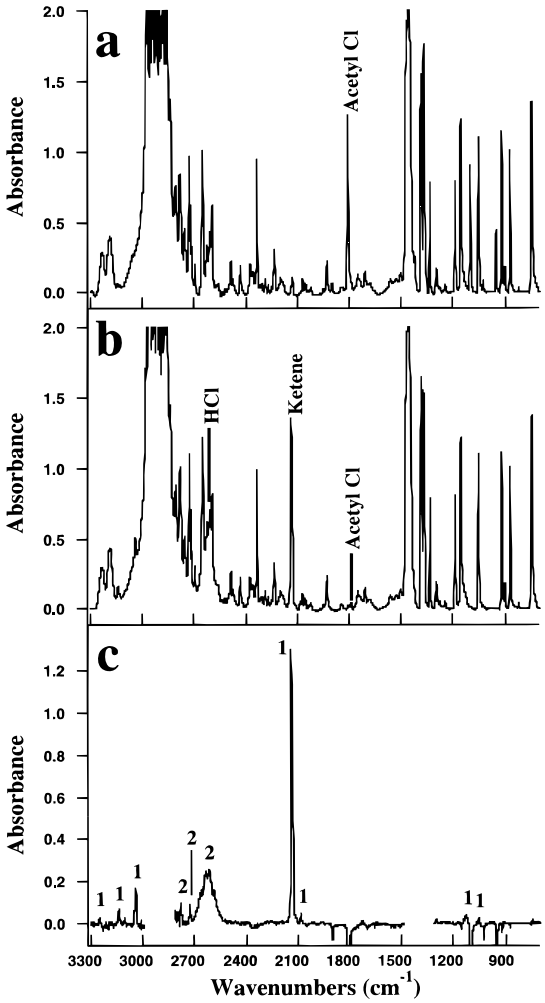

Figure 4. Preirradiated (a) and postirradiated (b) IR spectra of acetyl chloride matrix-isolated in propane (300:1 at 11 K). The loss of acetyl chloride and the production of HCl and ketene are observed following 266 nm irradiation. The difference spectrum (c) displays ketene (1) and HCl (2) IR bands. The whited out regions, near 1400 and 2900 cm^{-1}, correspond to offscale absorption by the IR bands of propane (CH_3 stretch and deformation modes).

Polarization Studies. Polarized FTIR spectra are analyzed by fitting the normalized integrated IR intensities of nonoverlapped vibrational modes to the functional form

$$I(\vartheta) = A[\cos^2(\vartheta + \phi) + \cos^2(\vartheta - \phi)] \qquad (10)$$

The variables A, ϑ, and ϕ represent the amplitude, angle of polarizer rotation, and orientation angle of the vibrational dipole, respectively. The orientation angle ϕ determines the average angle of a vibrational dipole about the z axis (the vertical laboratory axis). The difference of the maximum and minimum values of the normalized integrated intensities relates to the degree of product polarization and how closely a particular vibrational dipole is oriented to either the vertical or horizontal axis. The greatest differences in the integrated intensity are observed for well-aligned vibrational dipoles oriented parallel to the vertical or horizontal axis. The smallest differences are observed for well-aligned vibrational dipoles oriented near 45° or for isotropically distributed products.

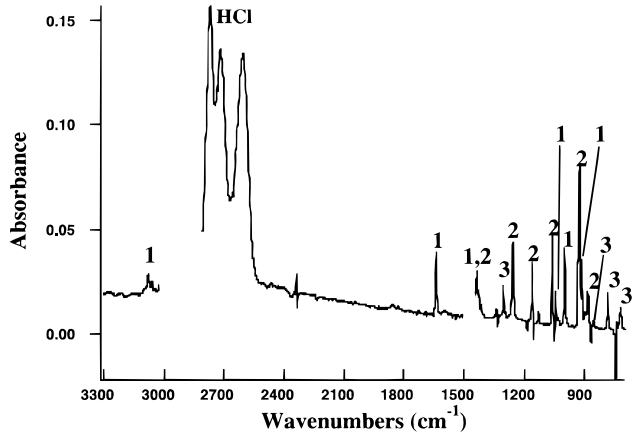

Figure 5. Difference spectrum of 355 nm irradiated Cl_2 isolated in a propane matrix (200:1 at 11 K). The observed photoproducts bands are attributed to HCl, propene (1), 2-chloropropane (2), and 1-chloropropane (3). The offscale CH_3 stretch and deformation bands of propane are whited out. None of these organic products are observed in the difference spectrum of 266 nm irradiated acetyl chloride in propane (Figure 4c).

TABLE 2: Vibrational Frequencies (cm^{-1}) of the Photoproducts of 193 nm Irradiated Acetyl Chloride in a Propane Matrix

assignments	observed frequency	literature frequency	mode
2-chloroethanol[a]	3315	3366	ν(OH)
propene	3086	3091	ν(CH)
acetaldehyde[b]	3008	3001	$\nu(CH_3)$
HCl	2799−2667		
ketene,[c] CO[d]	2148−2135	2133	ν(C═O)
		2137	
acetaldehyde	1725	1726	ν(C═O)
propene	1646	1646	ν(C═C)
2-chloroethanol	1300	1305	$\rho(CH_2)$
2-chloropropane	1260	1260	$\rho(CH_3)$
2-chloropropane	1165	1161	$\rho(CH_3)$
propene	992	992	ν(C−Cl)
propene, 2-chloropropane	933	934	$\rho(CH_2)$
		933	$\rho(CH_3)$
propene	910	910	$\delta(CH_2)$
2-chloropropane, cyclopropane[e]	867	885	ν(CC)
		867	ν(CC)
2-chloroethanol	735	749	ν(C−Cl)

[a] Frequencies of liquid 2-chloroethanol from ref 34; assignments from ref 37. [b] Frequencies of liquid acetaldehyde from ref 34; assignments from ref 38. [c] Solid ketene assignments from ref 31. [d] Matrix-isolated (argon) CO assignments from ref 39. [e] Gas-phase cyclopropane assignments from ref 40.

Figure 7 shows the fit of eq 10 to the integrated IR absorbance of ketene and HCl. We use the ketene C═O and the HCl stretch modes to determine molecular orientations relative to the vertically (*z* axis) polarized UV laser. Identical HCl·ketene photoproducts, with similar yields, are found in both argon and xenon matrixes. However, well-aligned products are observed in the argon matrixes while only slightly aligned species are observed in the xenon matrixes. These differences are likely due to the migration of HCl within the more open xenon matrix. Maximum values for the normalized integrated intensities are observed at 0° and 180° for HCl and 90° for ketene.

In Figure 8, the geometry of the HCl·ketene complex is compared to the transition-state structure from Sumathi and Chandra.[17] Orientation angles for the vibrational dipoles of HCl and ketene are obtained from the fit of the normalized IR intensity data with eq 10 (Figure 7) and yields an angle of ∼90°

TABLE 3: Vibrational Frequencies (cm^{-1}) of the Photoproducts of 193 nm Irradiated Acetyl Chloride in a Xenon Matrix

assignments	observed frequency	literature frequency	mode
methyl radical[a]	3153	3150	$\nu_{as}(CH)$
ketene	3145	3140	$\nu_{as}(CH)$
ketene	3047	3043	$\nu_s(CH)$
methyl radical	3006	3004	$\nu_s(CH)$
methyl chloride[b]	2951	2980	$\nu_s(CH_3)$
isolated HCl	2855		
semi-isolated HCl	2807		
complexed HCl	2661		
ketene, CO	2134	2133	ν(C═O)
		2137	
acetyl radical[c]	1874	1875	ν(C═O)
methyl chloride	1439	1458	$\delta_{as}(CH_3)$
ketene	1372	1374	$\delta(CH_2)$
methyl chloride	1345	1350	$\delta_s(CH_3)$
acetyl radical	1320	1329	$\delta_s(CH_3)$
ketene	1129	1131	ν(C═C)
methyl chloride	1016	1019	δ(C−Cl)
methyl chloride	728	732	ν(C−Cl)

[a] Matrix-isolated methyl radical assignments from ref 41. [b] Gas-phase methyl chloride assignments from ref 42. [c] Matrix-isolated acetyl radical assignments from ref 41.

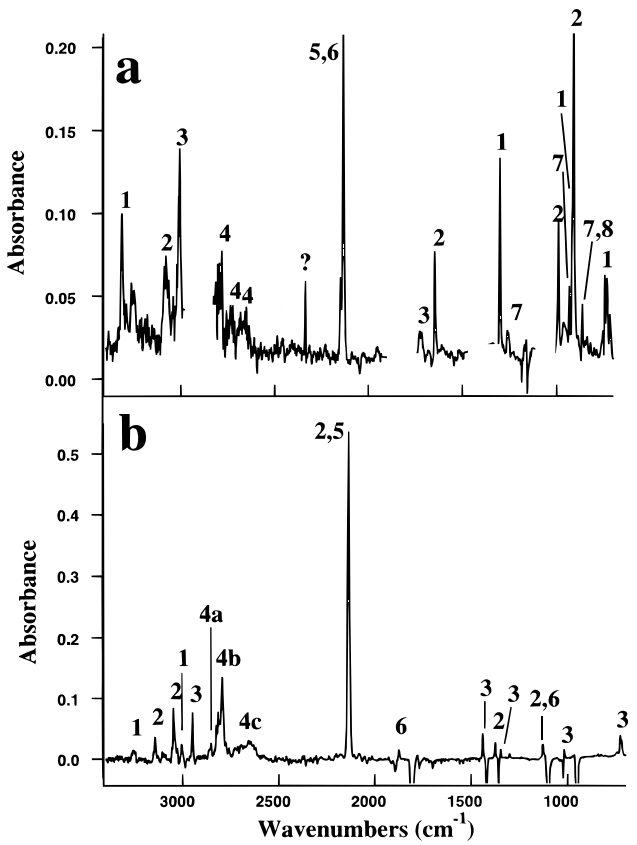

Figure 6. Difference spectrum (a) of acetyl chloride irradiated at 193 nm in a propane matrix (200:1 at 11 K). Vibrational bands are assigned to 2-chloroethanol (1), propene (2), acetaldehyde (3), HCl (4), ketene and CO (5 and 6), 2-chloropropane (7), and possible cyclopropane (8). The offscale CH_3 stretch and deformation bands of propane and acetyl chloride (including the CO stretch of acetyl chloride) are again whited out. The difference spectrum (b) of acetyl chloride irradiated at 193 nm in a xenon matrix (200:1 at 11 K) contains vibrational bands assigned to the methyl radical (1), ketene (2), methyl chloride (3), HCl (4), CO (5), and acetyl radical (6).

between the HCl and C═C═O molecular axis. On inspection, the experimental T-shaped structure is very similar to the calculated transition-state structure.

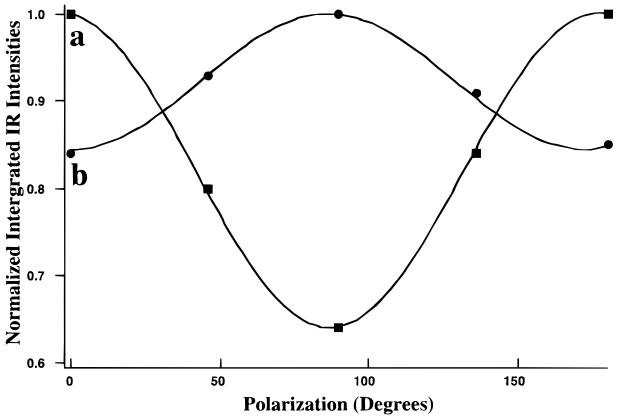

Figure 7. IR polarization dependence of the normalized integrated IR intensities of HCl (a) and ketene (C═O stretch) (b). The orientation angles are determined by fitting the polarization data with eq 10. Integrated intensity ratios were calculated by normalizing the IR absorption intensities to the largest integrated intensity for each vibrational mode. The 0° position of the IR polarizer is set to the vertical laboratory axis parallel to the polarization of the 266 nm laser. The IR spectra were taken at ~11 K for an irradiated deposit of matrix-isolated acetyl chloride (argon, 200:1).

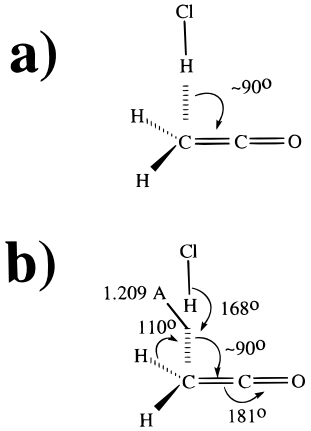

Figure 8. Proposed orientation of the HCl·ketene complex (a) compared with the transition-state geometry calculated in ref 17 (b).

Discussion

The S_1 UV photoexcitation of acetyl chloride in neat and matrix-isolated films yields only HCl and ketene as primary products. Several distinct mechanisms can be conceived from the processes described in reactions 2−9 that are consistent with this result. However, we argue that only one mechanism (mechanism I below) is consistent with all experimental observations:

mechanism I

$$[CH_3COCl] + h\nu \rightarrow [CH_3COCl\ (S_1)] \quad \text{(photoexcitation)} \tag{1}$$

$$[CH_3COCl\ (S_1)] \rightarrow [CH_3COCl^{\#}\ (S_0)] \quad \text{(internal conversion)} \tag{6}$$

$$[CH_3COCl^{\#}\ (S_0)] \rightarrow [HCl + H_2C{=}C{=}O] \quad (S_0 \text{ elimination}) \tag{8}$$

We find that the rapid dissociation of the C−Cl bond observed in the gas-phase reaction is not involved in the condensed-phase reaction, nor is any radical an intermediary. Although mechanisms II and III below initially appear plausible, the experimental results do not support initial dissociation of the C−Cl bond that is required by these mechanisms.

mechanism II

$$[CH_3COCl\ (S_1)] \rightarrow [Cl_t + H_3CCO^{\#}] \quad \text{(caged dissociation)} \tag{2}$$

$$[Cl_t + H_3CCO] \rightarrow [HCl + H_2C{=}C{=}O] \quad \text{(abstraction/disproportioantion)} \tag{3}$$

mechanism III

$$[CH_3COCl\ (S_1)] \rightarrow [Cl_t + H_3CCO^{\#}] \quad \text{(caged dissociation)} \tag{2}$$

$$[Cl_t + H_3CCO] \rightarrow [CH_3COCl^{\#}\ (S_0)] \quad (S_0 \text{ recombination}) \tag{5}$$

$$[CH_3COCl\ (S_0)] \rightarrow [HCl + H_2C{=}C{=}O] \quad (S_0 \text{ elimination}) \tag{8}$$

Furthermore, the experimental results do not support a mechanism involving an intermediary triplet state as described by mechanism IV:

mechanism IV

$$[CH_3COCl\ (S_1)] \rightarrow [CH_3COCl\ (T_1)] \quad \text{(intersystem crossing)} \tag{7}$$

$$[CH_3COCl\ (T_1)] \rightarrow [HCl + H_2C{=}C{=}O]^3 \quad (T_1 \text{ elimination}) \tag{9}$$

The evidence supporting mechanism I includes the singular primary reaction products, the highly favored elimination reaction path calculated for the ground electronic state,[17] the observed alignment of the reaction products, and the strong similarities between the determined structure of the HCl·ketene complexes and the calculated transition-state structure.[17] The experimental evidence against mechanisms II−IV also provides support for mechanism I owing to the limited number of possible reactions mechanisms available in the formation of HCl and ketene products.

Singular Reaction Products. Following 266 nm photoexcitation, several possible reactions are thermodynamically accessible, yet only HCl·ketene products are observed. The HCl·ketene products are observed in rare gas matrixes, in neat films, and even in propane and O_2 matrixes. These facts argue strongly that a single reaction mechanism is operative in the 266 nm condensed-phase photochemistry and that a direct dissociation of the C−Cl bond does not occur. This result is surprising considering the prompt ($\tau \approx 1$ ps) gas-phase dissociation. For the sake of argument, we will postulate that the first step following 266 nm excitation is prompt dissociation of the C−Cl bond and then consider the subsequent reaction mechanisms consistent with formation of the observed products.

In a rare-gas matrix the ejected Cl and acetyl radicals will be quickly "caged" and may then undergo H-atom abstraction/disproportionation (as described by mechanism II) or recombination (as described by mechanism III). If abstraction/disproportionation is the next reactive step, then the Cl atom must select among the three H atoms. On the other hand, displacement of CO to form CH_3Cl, reaction 4, would be quite plausible because the C−C bond in the acetyl radical is much

weaker than the C−H bond. The C−C bond strength of the acetyl radical is only 11.4 kcal/mol[10] (with a barrier of 17 kcal/mol), while the C−H bond strength is over 3 times larger at 42 kcal/mol.[44] The enthalpy of formation for $CH_3Cl + CO$ from CH_3COCl is +12.2 kcal/mol, which is lower than the formation enthalpy for $H_2CCO + HCl$ at +25 kcal/mol.[45] Therefore, a CO displacement reaction to form CH_3Cl is favored on thermodynamic grounds. However, no IR band attributable to CH_3Cl is observed, and the signal-to-noise displayed in Figure 2 clearly limits any formation of CH_3Cl to less than 1% of the reaction products. Reaction 4 is therefore nonoperative.

If recombination of CH_3CO with Cl on the S_0 surface is the next reactive step, then a four-center elimination reaction may follow (mechanism III). Mechanism III is distinctly different from our favored mechanism I and must satisfy some very unlikely requirements. (1) Every dissociated Cl and acetyl radical geminate pair must be caged and recombine. No displacement reaction may occur because (by the above arguments) CH_3Cl and CO would then be observed. (2) The ejected Cl atom must be uncharacteristically unreactive toward the propane matrix. The gas-phase reaction of Cl with propane proceeds at essentially the collision rate (1.4×10^{-10} cm^3 molecule^{-1} s^{-1}) and is independent of temperature over the range 292−800 K.[46] If a hot Cl atom is first ejected from acetyl chloride within a propane matrix, one would expect to observe HCl, propene, chloroethanes, acetaldehyde, methyl propyl ketone, acetyl radical, and CO products. However, no such bands are identified in the IR spectrum of the irradiated sample at 266 nm.

The 355 nm irradiation of Cl_2 isolated in a propane matrix produces propene ($H_2C{=}CHCH_3$), 2-chloropropane, and 1-chloropropane, clearly indicating reaction of Cl with the cryogenic propane matrix. None of these photoproducts, CO, or acetaldehyde is observed in the 266 nm photolysis of acetyl chloride in propane. By our measurements, the reaction yield for Cl of acetyl chloride with the propane matrix must be less than 1%. This is a very low probability for a reaction that appears to occur on *every collision* in the gas phase. Similarly, ClOO is not observed for acetyl chloride irradiated in an O_2 matrix.

The 193 nm photoexcitation[47] of the acetyl chloride S_2 state, however, leads to reactions characteristic of Cl-atom dissociation. Propene, 2-chloropropane, 2-chloroethanol, HCl, acetaldehyde, and CO products are observed following 193 nm irradiation of CH_3COCl in a propane matrix. Similar products, such as propene and 2-chloropropane, are also observed following 355 nm excitation of Cl_2 isolated in propane. Furthermore, 193 nm excitation of CH_3COCl in a xenon matrix leads to formation of CH_3, CO, CH_3Cl, and the acetyl radical, i.e., the reaction products expected from mechanisms II and III. Therefore, under 193 nm irradiation, cage escape of chlorine atoms occurs in a xenon matrix. These results again demonstrate that the reactions typical of Cl radicals readily occur in cryogenic propane and xenon matrixes.

Photoproduct Alignment. Following concerted elimination (mechanism I), we expect the photoproducts to be aligned relative to the polarization of the irradiating laser. It is less likely that photoproducts produced by a stepwise abstraction/disproportionation reaction (mechanism II) will be aligned because a Cl atom could react with any of the three methyl hydrogens of the acetyl radical. We observe that the HCl·ketene complexes are well aligned in the neat and Ar matrix-isolated samples. Only weak alignment is observed for HCl·ketene complexes in the Xe matrix. This is attributed to the larger openings of the Xe matrix that allow movement and possible cage escape of the photoproducts.

The orientation of the HCl perpendicular to the molecular axis of ketene is thought to occur for several reasons. Mulliken analysis indicates that the methylenic carbon has the largest anionic charge in the ketene molecule and thus attracts the H atom of the hydrogen chloride. During the concerted elimination reaction, the C−Cl bond becomes highly stretched and finally removes an H atom from the methyl group at a nearly T-shaped transition state.[17] The HCl hydrogen simply remains trapped near the methylenic carbon in the dimer product configuration. Since the hydrogen interacts most strongly with the methylenic carbon, the chlorine atom is located such that the H−Cl bond axis is nearly perpendicular to the O=C=C bond axis of ketene. A comparison of the dimer and transition-state structure is presented in Figure 8.

Ultraviolet Photomechanism. The gas- and condensed-phase photoreaction of acetyl chloride are markedly different! In the gas phase the C−Cl bond is rapidly broken, forming a Cl atom and acetyl radical that may subsequently dissociate into CH_3 and CO. The subpicosecond time scale for the gas-phase C−Cl bond dissociation has been determined from measurements of the Cl photofragment anisotropy[8−10] and by femtosecond real-time clocking.[11] The rapid ejection of the Cl atom is attributed to the transformation of the initial excited $^1[n,\pi^*(C{=}O)]$ state into a repulsive excited state $^1[n,\sigma^*(C{-}Cl)]$ on the singlet excited surface.[8,14−16] The time scale for C−Cl bond breaking is so short that it is inconceivable that the condensed-phase process could occur much more rapidly. The signal-to-noise of our measurements limits the contribution of C−Cl dissociation to less than 1% in the condensed phase. Therefore, if the condensed-phase mechanism is simply more rapid than the gas-phase dissociation, then the time scale for mechanism I is on the order of 10 fs—a clearly unreasonable conclusion. We conclude that the presence of the surrounding matrix must impede the transformation of the initial excited state into a repulsive state.

We attribute the change in the photodissociation mechanism to the intermolecular interactions of the acetyl chloride with the surrounding matrix. These interactions most likely shift (perturb) the relevant excited states such that the coupling of the initial excited state to the final repulsive state is slowed well beyond the interconversion time scale. The couplings of the avoided crossing(s) must be very sensitive to third-body perturbations because we observe mechanism I in all matrix materials. It may be possible to probe the excited-state lifetime of matrix-isolated acetyl chloride by time-resolved luminescence measurements. Ab initio electronic structure calculations of rare gas/acetyl chloride clusters may be necessary to determine the nature of the perturbation of the avoided crossing(s).

We discount any role of S_1-to-T_1 intersystem crossing in the reaction mechanism because the photodissociation efficiencies in irradiated Ar and Xe matrixes are identical. Xenon is known to promote intersystem crossing by the heavy atom effect,[48] yet little change in reaction yield is observed. And although oxygen is an efficient triplet quencher, the quantum efficiencies for photolysis of acetyl chloride in an O_2 matrix is at least as great as in an argon matrix. The calculation of Sumathi and Chandra reveals several low-barrier (8−14 kcal/mol on the lowest adiabatic triplet surface) reaction paths leading to radical products. If S_1-to-T_1 intersystem crossing is a significant channel, then cleavage of the C−C and C−Cl bonds and the formation of CH_3, COCl, and CH_3CO molecules would be predicted.[8] Since CH_3 and COCl products are not observed, nor are any products attributed to radicals, we conclude that the dissociation pathway proceeds on the ground-state electronic surface following $S_1 \rightarrow S_0$ interconversion.

Conclusions

Photoexcited samples of condensed-phase acetyl chloride react on the ground electronic state surface by HCl elimination following $S_1 \rightarrow S_0$ interconversion (mechanism I). We conclude that intersystem crossing $S_1 \rightarrow T_1$ leading to reaction from the lowest triplet state does not occur because of the similar quantum yields observed in Ar, Xe, and O_2 matrixes and because no radical products are observed. We find identical reaction products following 266 nm irradiation of acetyl chloride molecules in neat, Ar, Xe, O_2, and propane matrix-isolated thin films.

Our data do not support either geminate recombination or stepwise caged abstraction mechanisms (mechanisms II and III). The observation of alignment of the HCl·ketene complexes relative to the polarization axis of the irradiating laser, the lack of CH_3Cl, and acetyl radical products in the xenon matrixes are contrary to the expectations of a caged abstraction mechanism. The only observed primary photoproducts are HCl·ketene complexes in all matrixes reported here. The lack of propene, acetaldehyde, and chloropropanes for irradiation of acetyl chloride isolated in propane indicates that the Cl atom is not ejected following photoexcitation. These facts eliminate all possible photodissociation mechanism except the four-center direct elimination mechanism (mechanism I).

The determined geometry of the HCl·ketene complex is oriented such that the bond axis of HCl is approximately 90° to the ketene symmetry axis, with the hydrogen of HCl interacting with the methylenic carbon of ketene. This structure is very similar to the calculated transition-state structure for HCl elimination.[17]

Acknowledgment. The authors were supported by the Division of Chemical Sciences of the Office of Basic Energy Sciences, U.S. Department of Energy. Pacific Northwest National Laboratory is operated for the U.S. Department of Energy by Battelle under Contract No. DE-AC06-76RLO 1830. We also thank Professor G. Barney Ellison and Paul Winter for stimulating discussions.

References and Notes

(1) Molina, M. J.; Tso, T.; Molina, L. T.; Wang, F. C. Y. *Science* **1987**, *238*, 1253.
(2) Zhang, R.; Jayne, J. T.; Molina, M. J. *J. Phys. Chem.* **1994**, *98*, 867.
(3) *Chem. Eng. News* **1994**, *August 15*, 8.
(4) Tielens, A. G. G. M.; Allamandola, L. J. In *Physical Processes in Interstellar Clouds*; Morfill, G. E., Scholer, M., Eds.; Reidel: Dordrecht, 1987; p 333.
(5) Buch, V. In *Molecular Astrophysics*; Hartquist, T. W., Eds.; Cambridge University Press: Cambridge, 1990; p 132.
(6) Turro, N. J. *Modern Molecular Photochemistry*; University Science Books: Sausalito, CA, 1991.
(7) Rowland, B.; Hess, W. P. *Chem. Phys. Lett.* **1996**, *263*, 574.
(8) Person, M. D.; Kash, P. W.; Butler, L. J. *J. Chem. Phys.* **1992**, *97*, 355.
(9) Person, M. D.; Kash, P. W.; Butler, L. J. *J. Phys. Chem.* **1992**, *96*, 2021.
(10) Deshmukh, S.; Myers, J. D.; Xantheas, S. S.; Hess, W. P. *J. Phys. Chem.* **1994**, *98*, 12535.
(11) Shibata, T.; Suzuki, T. *Chem. Phys. Lett.* **1996**, *262*, 115.
(12) Deshmukh, S.; Hess, W. P. *J. Chem. Phys.* **1994**, *100*, 6429.
(13) North, S.; Blank, D. A.; Lee, Y. T. *Chem. Phys. Lett.* **1994**, *224*, 38.
(14) Sumathi, R.; Chandra, A. K. *J. Chem. Phys.* **1993**, *99*, 6531.
(15) Martin, X.; Moreno, M.; Lluch, J. M. *J. Phys. Chem.* **1993**, *97*, 12186.
(16) Martin, X.; Moreno, M.; Lluch, J. M. *J. Chem. Soc., Faraday Trans* **1996**, *92*, 373.
(17) Sumathi, R.; Chandra, A. K. *Chem. Phys.* **1994**, *181*, 73.
(18) Maccoll, A. *Chem. Rev.* **1969**, *69*, 33.
(19) Benson, S. W.; Bose, A. N. *J. Chem. Phys.* **1963**, *39*, 3463.
(20) Srivatsava, A.; Arunan, E.; Manke, G.; Setser, D. W.; Sumathy, R. Manuscript in preparation.
(21) Toto, J. L.; Pritchard, G. O.; Kirtman, B. *J. Phys. Chem.* **1994**, *98*, 8359.
(22) Biernacki, P. R.; Kaszynski, P.; Hess, B. A.; Thulstrup, E. W.; Radziszewski, J. G. *J. Phys. Chem.* **1995**, *99*, 6309.
(23) Arnold, B. R.; Balaji, V.; Downing, J. W.; Radziszewski, J. G.; Fisher, J. J.; Michl, J. *J. Am. Chem. Soc.* **1991**, *113*, 2910.
(24) Berg, O.; Ewing, G. E. *Surf. Sci.* **1989**, *220*, 207.
(25) Kobayashi, Y.; Ogino, T. *Surf. Sci.* **1996**, *100*/*101*, 407.
(26) Thulstrup, E. W.; Michl, J. *Elementary Polarization Spectroscopy*; VCH Publishers: New York, 1989.
(27) Groner, P.; Stolkin, I.; Gunthard, H. H. *J. Phys. E* **1973**, *6*, 122.
(28) *The Photonics Design and Applications Handbook*; Laurin Publishing: Pittsfield, MA, 1994.
(29) Sinnock, A. C. *J. Phys. C* **1980**, *13*, 2375.
(30) During, J. R.; Davis, J. F.; Guirgis, G. A. *J. Raman Spectrosc.* **1994**, *25*, 189.
(31) Moore, C. B.; Pimentel, G. C. *J. Chem. Phys.* **1963**, *38*, 2816.
(32) Kunttu, H. M.; Seetula, J. A. *Chem. Phys.* **1994**, *189*, 273.
(33) Ransley, I. A.; Ilharco, L. M.; Bateman, J. E.; Sakakini, B. H.; Vickerman, J. C.; Chesters, M. A. *Surf. Sci.* **1993**, *298*, 187.
(34) Pouchert, C. J. *The Aldrich Library of FT-IR Spectra*; Aldrich Chemical Co: Milwaukee, WI, 1985; Vols. 1 and 2.
(35) Brown, J. K.; Sheppard, N. *Trans. Faraday Soc.* **1954**, *50*, 1164.
(36) Klaboe, P. *Spectrochim. Acta* **1970**, *26*, 87.
(37) Perttila, M.; Murto, J.; Halonen, L. *Spectrochim. Acta* **1978**, *34*, 469.
(38) Hisatsune, I. C. *Spectrochim. Acta* **1983**, *39*, 853.
(39) Maki, A. C. *J. Chem. Phys.* **1961**, *35*, 931.
(40) Herzberg, G. *Molecular Spectra and Molecular Structure II. Infrared and Raman Spectra of Polyatomic Molecules*; Van Nostrand Reinhold: New York, 1945.
(41) Jacox, M. J. *Vibrational and Electronic Energy Levels of Polyatomic Transient Molecules*; American Institute of Physics: Woodbury, NY, 1994.
(42) Rasko, J. R.; Bontovics, J.; Solymosi, F. *J. Catal.* **1993**, *143*, 138.
(43) Kogure, N.; Ono, T.; Suzuki, E.; Watari, F. *J. Mol. Struct.* **1993**, *296*, 1.
(44) Berkowitz, J.; Ellison, G. B.; Gutman, D. *J. Phys. Chem.* **1994**, *98*, 2744.
(45) *Handbook of Chemistry and Physics*, 75th ed.; CRC Press: Boca Raton, FL, 1995.
(46) Pilgrim, J. S.; McIlroy, A.; Taatjes, C. A. *J. Phys. Chem. A* **1997**, *101*, 1873.
(47) Maricq, M. M.; Szente, J. J. *Chem. Phys. Lett.* **1994**, *220*, 243.
(48) Laursen, S. L.; Pimentel, G. C. *J. Phys. Chem.* **1990**, *94*, 8175.